Chapter

Analysis of the Tribological Evolution of Nitride-Based Coatings

Christian Ortiz Ortiz, Erick Hernandez-Rengifo and Julio Cesar Caicedo

Abstract

This chapter describes the fundamental and technological role of nitride-based hard coatings as protective coatings in some applications within the metalworking industry. For this, this chapter will present a critical review of previous research and recent developments on nitride-based coatings in different systems such as (multilayers, quaternaries, among others), where it will be possible to demonstrate their main properties and advantages that they can grant when they are implemented on conventional steels, such as greater hardness, surface control, electrochemical resistance, resistance against wear, among others. These results will determine that this type of coatings are suitable candidates to be implemented as protective coatings on cutting tools, which suffer from high wear in machining processes in the metalworking industry.

Keywords: tribology behavior, wear mechanisms, multilayer coatings, adhesive properties, surfaces analysis

1. Introduction

Through constant development within the metalworking industry, current processes consist of designing and producing new structures at a higher speed, cheaper with more efficient processes that present a low rate of wear on the equipment and devices used during said processes. Therefore, hard wear-resistant coatings have been incorporated as protective coatings on cutting tools in recent decades with the purpose of giving a longer useful life to this type of device, which suffers from high wear during the machining processes [1–3]. This type of coatings currently has a wide range of investigations, which have been able to generate different configurations such as binary, ternary or quaternary systems, single or multilayer systems, as well as a great combination of different elements that have conferred characteristics. Special to this type of coatings, such as high hardness, high biocompatibility, high resistance to wear, high resistance to corrosion, among other specific characteristics required depending on their use and application. A specific type of coatings such as those based on nitrides, which have generated great interest within various and novel coating systems, these coatings were implemented approximately since 1970 [4], being one of the first anti-wear coatings used in the industry. This type of coatings have great hardness, high resistance to wear and high resistance to

corrosion among other interesting properties, such as TiN [4], TiCrN [5], [Al_2O_3/Si_3N_4] [6], TiCN [7], BCN [8] among other configurations.

Nitride-based coatings are constituted by the incorporation of nitrogen atoms (N) within the crystalline structure of transition metals such as Ti, Al, Cr, V among others, which generates a distortion within their structure, causing internal stresses, with changing specific properties of the material. In addition, the inclusion of N atoms interstitially within the structures generates a physicochemical change in the material, giving it changes in its behavior based on a new metal-ceramic structure that it now presents. Therefore, properties such as hardness and corrosion resistance increase considerably in relation to simpler coatings based on transition metals. On the other hand, the distortion within their structures due to the inclusion of N atoms generating stresses within their structure as mentioned above, causes physical changes in the coating, such as an increase in the density of these coatings, which influences characteristics. Surface surfaces such as roughness and the presence of these residual stresses within the structure, causes an increase in the mechanical properties of the coating, among other changes in material properties.

2. Methodology and experimental details

The deposition of the coatings was performed using a multi-target sputtering magnetron. This specific type of system allows to perform the multilayer deposition process in situ. This equipment uses four (4) magnetrons (Torus - 4 “, 10 cm Kurt J. Lesker) with diameters of 10 cm, three (3) radio frequency sources (13.56 MHz, RFX 600A), and three (3) direct current sources (MDX 500, Advanced Energy). In addition, the pressure during the deposition process in monitored by a control and measurement system (Baraton, MKS), which has four (4) gas flow controllers, a radiation heating system (Athena 500), which has a maximum temperature of 400°C, and a planetary type rotary sampling system. For TiN, TiCrN, TiCN, BCN and CrAlN coatings, titanium (Ti), titanium carbide (TiC) and Chromium-Aluminum (Cr-Al) targets were used, respectively; each cathode with an approximate purity of 99.99%. Two (2) different type of substrate were used, silicon with preferential crystallographic orientation (100) and AISI 1045 and H13 steel substrates respectively. The silicon substrates were subjected to a surface cleaning process in an ultrasonic system and the steel substrates were prepared superficially using sandpaper (SiC) and finally polished in a metallographic polisher. Before starting the deposition process, a vacuum with a pressure of $1.4x10^{-4}$ mbar was applied. The TiCN coating was deposited using a working pressure of $1.4x10^{-2}$ mbar in a gas mixture of 50 sccm (Ar) and 16 sccm (N_2) at 250°C, and a r.f power density of 5 W/cm^2 was applied on the TiC target. For BCN coating, it was deposited by a pressure of $7.4x10^{-3}$ mbar in a gas mixture of 44 sccm (Ar) and 6 sccm (N_2) at 250°C, and a r.f power density of 7 W/cm^2 was applied on the BC target. For the CrAlN coating was deposited using a working pressure of $6.4x10^{-3}$ mbar was used a gas mixture of 50 sccm (Ar) and 5.5 sccm (N_2) at 250°C, and the r.f power density applied to the Cr target and Al target was 2.5 W/cm^2 and 4.5 W/$cm^{2,}$ respectively [8]. The deposition of the Si_3N_4 based coatings was performed by magnetron sputtering with an r.f source (13.56 MHz) on silicon (100) and AISI 316 stainless steel substrates. A cathode (Si_3N_4) with a purity of 99.9% approximately. During the deposition a power of 550 W was used and a bias voltage of −20 V was applied, the distance between substrates-targets was approximately 7 cm, and the deposition process was carried out at a temperature of 200°C inside the chamber. In addition, the substrate holder rotated at a

speed of 60 RPM during the entire deposition process with a working pressure of $5.1x10^3$ mbar. The coating obtained a thickness of approximately 2.5 μm.

The structural analysis of TiCN, BCN and CrAlN coatings was analyzed by X-ray diffraction (PANalytical X 'pert proTM), using a Cu Kα radiation source with a wavelength of λ = 1.5405 Å. By X-ray photo-electron spectroscopy (XPS) using a SAGE HR100 (SPECSTM) equipment with a monochromatic source (Mg Kα 1253.6 eV), CasaXPS V2.3.15 software was used to determine the chemical composition of the obtained coatings. The morphological study of the coatings was carried out by atomic force microscopy (AFM) with an Asylum Research MFP-3D® device and with a scanning prove image processor (SPIP®), the grain size and roughness of the coatings obtained were calculated. The mechanical study was carried out by nanoindentation using an Ubi1-HysitronTM device, which uses a Berkovich diamond tip at variable loads. From this test, load–displacement curves were obtained as a function of penetration for the coatings. Based on these curves, hardness and elastic modulus were determined using the Oliver-Phar method.

2.1 Tribological experimental details

The tribological characterization of the coatings was performed under ASTM G99-17 standard, using a Microtest MT 4001-98 tribometer. This equipment consists of a rotating platform, with controlled speed on which the test sample is adjusted in an environment with or without lubricant. On this surface, a mechanical arm which contains a counterpart (100Cr6 or Steel 440) with a spherical shape of 6 mm in diameter in direct contact with the surface under study is adjusted. A load applied to the counterpart (5 N) is adjusted on this mechanical arm; with an angular velocity of 160 rpm and linear velocity of 0.1 m/s and other parameters of each tribological test are presented in **Table 1**. In addition, a JEOL model JSM-6490LVTM scanning electron microscopy (SEM) was used to observe the wear track. The adhesive characterization of the coatings was performed under ASTM G171-03 standard, using a Microtest MTR2 equipment, the parameter used in the test were; a sliding distance of 6 mm, variable load from 0 to 90 N and a sliding velocity of of 1.97 mm/min using a Rockwell C indenter. In addition, the identification of cohesive failure (Lc1) and adhesive failure (Lc2) was performed using the NANOVEA SCRATCH TESTER software, which analyzes the change of the friction coefficient versus load or distance, and the results were corroborated by optical micrographs and SEM micrographs of the scratch tracks. The coatings thickness and the wear scratch images were obtained by using a KLA Tencor D-120 profilometer; the thickness of all the coatings was 3 μm [6, 9].

	TiN, TiCrN	**TiCN, CrAlN, BCN**	**Si_3N_4**
Load (N)	5	5	5
Counterpart	440	100Cr6	100Cr6
Environments	dry	Dry and lubricated	Dry and lubricated
Substrate	Steel H13	Steel 1045	Steel 316
Distance (m)	100	1000	300
Lubricant		20 W50	20 W50
Angular Velocity (rpm)	160	160	160
Linear Velocity (m/seg)	0.1	0.1	0.1

Table 1.
Tribological parameters.

3. Comparison between nitride coatings

3.1 Structural study for TiN and TiCrN nitride coatings

Figure 1 shows the diffraction patterns for the initial coating based on (TiN), where diffraction peaks located in the crystallographic planes (111) (200, 220), (311), (222) and (400) were obtained. In addition, the incorporation of Cr atoms within its structure for the formation of the coating (TiCrN), which still shows the same characteristics peaks. On the other hand, the displacement of the characteristics peaks of the multilayer system formed by [TiN/TiCrN] can be evidenced as a function of the increase in the bilayers number deposited on Si substrates (100). Determining that the increase in the number of interfaces causes a distortion of the crystalline structure due to residual stresses within this multilayers system, which will influence the mechanical and tribological properties of this type of coatings. From these results it was possible to infer that all coatings have a face-centered cubic crystal structure (FCC) [5, 10].

3.1.1 Structural study for TiCN, BCN and CrAlN coatings nitride coatings

Figure 2 shows the X-ray diffraction patterns for more complex coatings such as TiCN, BCN and CrAlN coatings. From these results, 2θ diffraction sequences were evident for face-centered cubic (FCC), NaCl type structures with and Fm3m space group [11]. The conformation of this type of coatings (TiCN, BCN and CrAlN) is associated by the substitution mechanism, in which, the carbon atoms (C) substitute the nitrogen atoms (N), giving rise the ordered CN systems in Ti, B and unordered for TiCN and BCN coatings. On the other hand, the CrAlN coating is the result of the coupling the two FCC phases of AlN and CrN, which generated a conjugated complex, where Al and Cr atoms are located in reticular positions and aluminum atoms (Al) are substituted by atoms of (Cr) while nitrogen atoms are located in the interstitial position of the CrAlN crystal [12–14]. Through these results, a NaCl-type FCC structure was determined for the three coatings, in which Ti, B, Cr and Al atoms would be located at the Wyckoff 4a site and the Wyckoff 4b site is randomly occupied by C and N atoms. Thus, titanium carbon-nitride as well as boron carbo-nitride are agreement with the international indexing files JCPDF 00-042-1488 and JCPDF

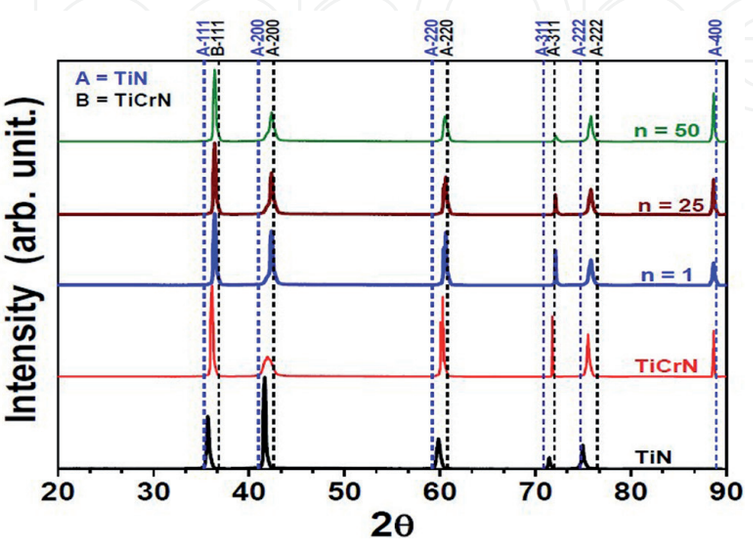

Figure 1.
X-ray diffraction patterns for monolayers [TiN and TiCrN] and multilayers [TiN/TiCrN]n as a function of the number of bilayers 1, 25, and 50.

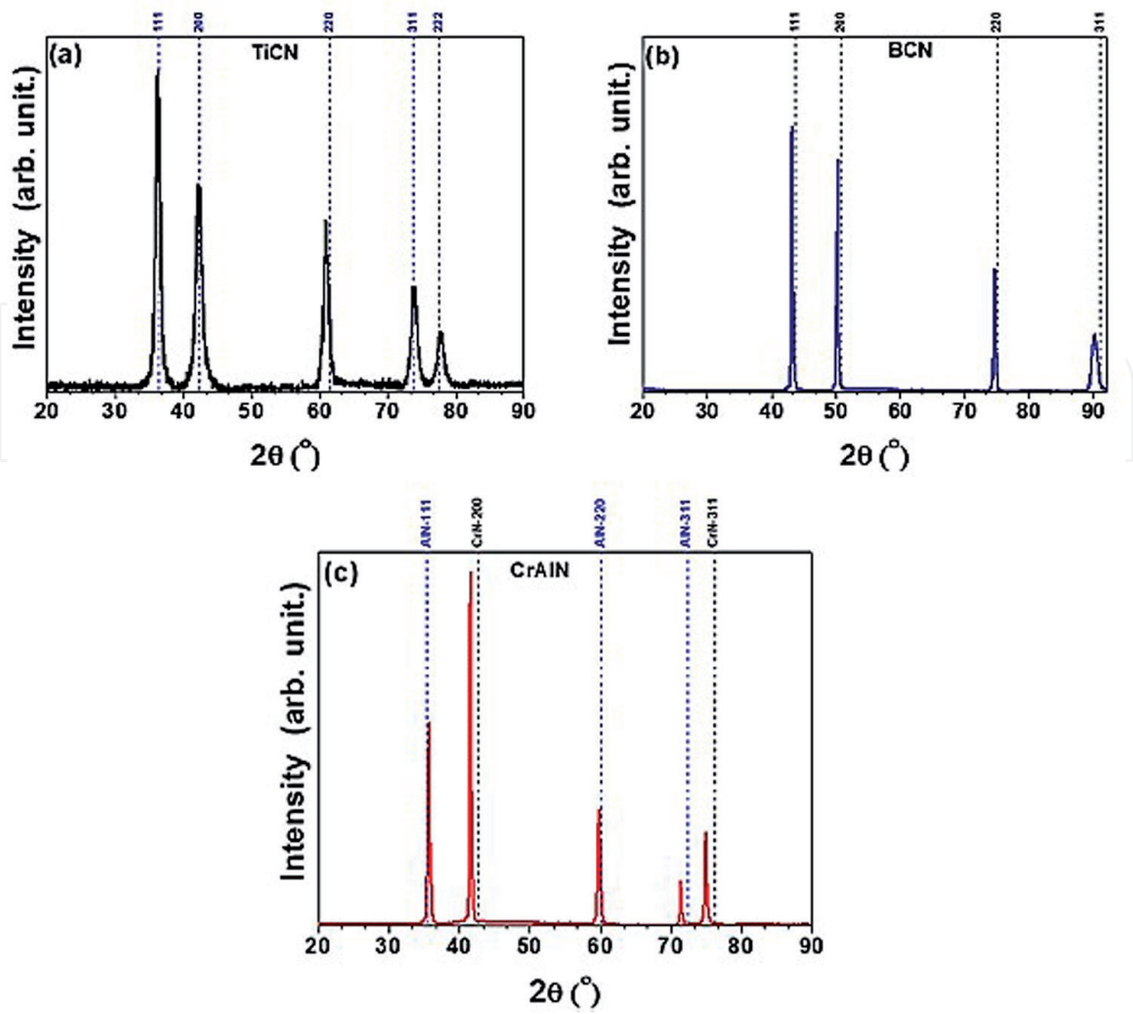

Figure 2.
Diffraction patterns for all coatings: (a) TiCN, (b) BCN and (c) CrAlN. Dotted lines indicate the peaks position obtained from the international indexing files (JCPDF) of TiCN, BCN and CrN–AlN respectively.

00-035-1293, while for aluminum chromium nitride two indexing are performed, taking into account the structure of chromium nitride (CrN) JCPDF 00-003-1157 and aluminum nitride (AlN) JCPD 00-025-1495 [15]. In addition, it can be observed that the CrAlN coating is constituted by CrN and AlN, which present the same NaCl-type FCC crystal structure and a 225-Fm3m space group. These results established that the higher intensity peak (111) located at the for angles 2θ = 36.342° and 43.228° for TiCN and BCN coatings respectively. Otherwise, for the CrAlN coating, where the peak of higher intensity (200) was located at angle 2θ = 41.646°. Finally, shifts towards smaller 2θ angles relative to the positions where the material is stress-free (dotted line). These shifts of the diffraction peaks suggest a variation of the lattice parameter of the crystal structures of the coatings. Considering that TiCN, CrAlN and BCN coatings present cubic structures, it can be observed that when the value of the theta angle (θ) decreases, the lattice parameter increases, evidencing an increase of the internal stresses (compression type) within the crystalline structure of the coatings.

3.1.2 Structural study for Si_3N_4 nitride coatings

Figure 3 shows the XRD diffraction patterns for Si_3N_4 coating deposited on silicon (100), where diffraction peaks located in the (111), (220), (311), (400), (511), (440) and (533) crystallographic planes characteristics of a face-centered cubic structure FCC were obtained. In addition, a preferential texturization is observed in the (311)

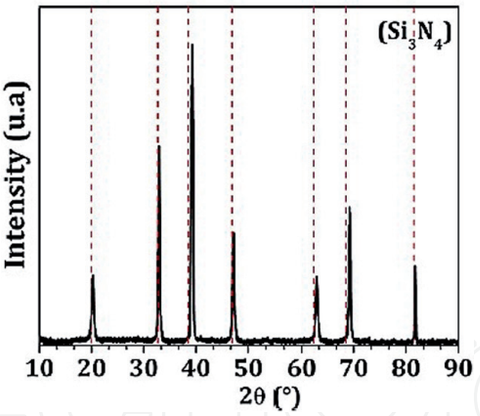

Figure 3.
Diffraction patterns of the Si_3N_4 single layers coating deposited on silicon.

plane, it was also observed that the peaks presented horizontal displacements at 2θ with respect to those reported in the JCPDC 00-051-1334 file (dotted line), were caused by internal stresses generated during the deposition process, which caused a deformation in the crystallographic planes of the structure of the coatings.

3.2 Chemical comparison between nitride coatings

3.2.1 Chemical study for TiCN, BCN and CrAlN coatings nitride coatings

Figure 4 shows the survey spectra for the TiCN, BCN and CrAlN coatings. These spectra presented high intensity peaks where their location with their

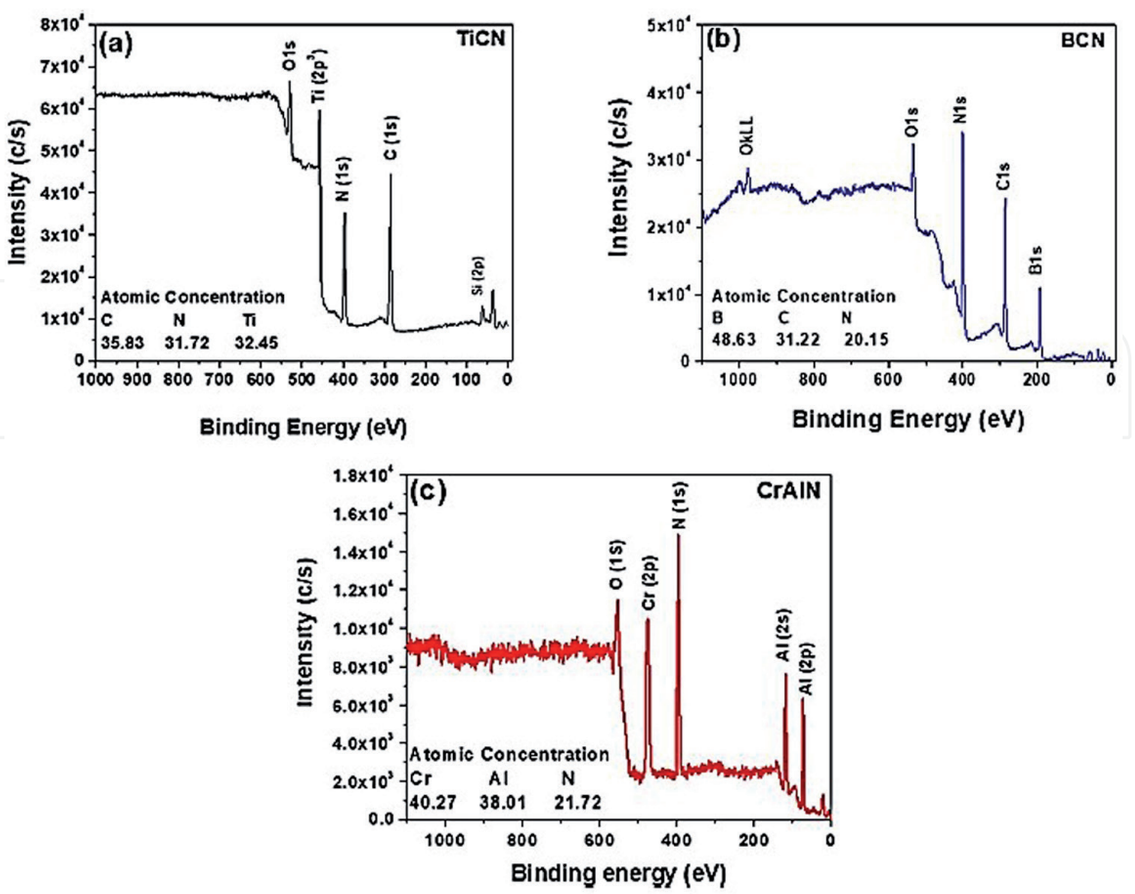

Figure 4.
XPS survey results for the three coatings used: (a) TiCN, (b) BCN and (c) CrAlN.

respective binding energies were determined. For the TiCN coating, Ti (2p3), C (1 s) and Si (2p) peaks located at the binding energy 458.4 eV; 396.8 eV; 284.8 eV and 61.6 eV respectively were obtained; for the BCN coating, N (1 s), C (1 s) and B (1 s) peaks located at the binding energy 400 eV; 285.6 eV and 192.8 eV respectively were obtained; and for the CrAlN coating Cr (2p), N(1 s), Al (2 s) and Al (2p) peaks located at the binding energy 475.99 eV; 396.97 eV; 119 eV and 74 eV respectively were obtained. Previous studies indicated that the signals of C (1 s) and N (1 s) are associated with C-N and Ti-N bonds, these results are agreement with the literature [16]. Analysis of the XPS spectra for the BCN coating showed the binding energies corresponding to the N (1 s), C (1 s) and B (1 s) signals were consistent to the formation of the BCN ternary compound as corroborated in the literature [17]. For the ternary CrAlN coating, Cr (2p3/2), Al (2p) and N (1 s) signals associated with Cr-Al bonds were presented, binding energies for Cr-N and Al-N were also evidenced, confirming the formation of the ternary CrAlN compound [18]. Finally, the stoichiometry was determined for all the coatings ($Ti_{32.45}$-$C_{35.83}$-$N_{31.72}$, $B_{48.63}$-$C_{31.22}$-$N_{20.15}$ and $Cr_{40.27}$-$Al_{38.01}$-$N_{21.72}$).

3.2.2 Chemical study for Si_3N_4 nitride coatings

Figure 5a show the depth spectra for the Si_3N4 coating, showing the spectral lines of the elements present in the coating by X-ray photoelectron spectroscopy (XPS) technique. From this result, elements such as Si and N, and elements in low quantity such as Oxygen were found. In order to know the detailed surface stoichiometry of the coating, the high resolution XPS spectra of Si-2p and N-1 s species are also presented in the **Figure 5b** and **c** respectively. The Si_3N_4 coating has an atomic N/Si ratio of 1.32 (stoichiometry $Si_{57}N_{43}$). The Si_3N_4 has an ideal stoichiometry ratio of 1.33 which is in agreement with what is found in the literature. In addition, the

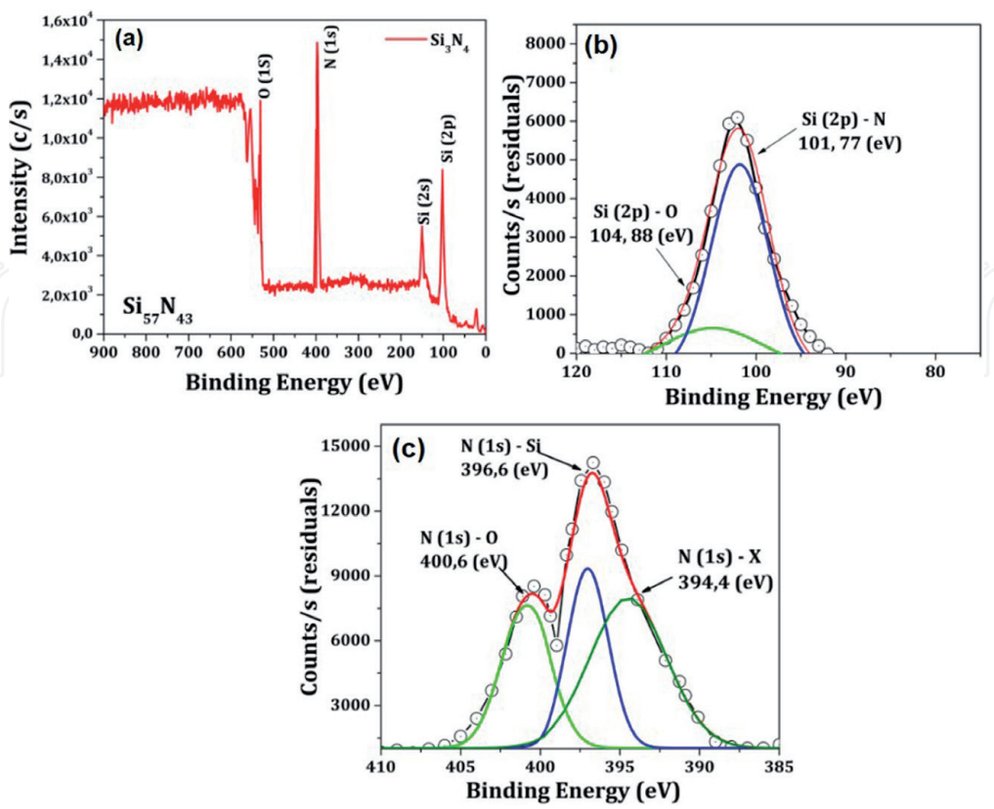

Figure 5.
Depth spectra obtained by the XPS technique for the Si_3N_4 nitride coatings and high resolution XPS spectra for the Si_3N_4 coating: (a) Si-2p signal; (b) N-1s signal.

high-resolution Si-2p spectrum (**Figure 5b**) presented two peaks located at a binding energy of 101.77 eV and 104.88 eV, respectively. These two peaks are attributed the Si-O and Si-N bonds of the Si_3N_4 [19]. On the other hand, **Figure 5c** shows the high-resolution spectrum for the N-1 s peak, which id fitted by three peaks. The first peak, corresponding to (N-O) bond, located at a binding energy 400.51 eV [20]; the second peak, corresponding to the (N-Si) bond, located at a binding energy of 396.96 eV, and the third peak, can be attributed to a different chemical state of N due to its different bonding configurations with neighboring atoms such as H and C located at a binding energy of 394.4 eV [21].

3.3 Morphological comparison between nitride coatings

3.3.1 Morphological study for TiN and TiCrN nitride coatings

To quantitatively study the surface morphology of the samples, the atomic force microscopy (AFM) technique was used. **Figure 6a** and **b** present the images corresponding to titanium nitride (TiN) and titanium chromium nitride (TiCrN) respectively. From these results, it was evident that the TiCrN surface has a more regular surface compared to TiN. This surface change is attributed to the incorporation of chromium (Cr) into its crystalline structure, which causes a compressive deformation, making a much denser and compact structure with a more orderly growth.

Figure 4c and **d** show the roughness and grain size for the TiN and TiCrN layers and the [TiN/TiCrN] based multilayer system as a function of the bilayers number n = 1, 25 and 50 respectively. These results indicated that the TiCrN layer presented better surface properties (roughness and grain size) compared to the TiN layer. In addition, by means of the multilayer system, it was evidenced that by increasing the bilayers number or interfaces, the surfaces presented a lower number of imperfections due to the fact that the system becomes much denser generating a more regular surface, because an increase in the density of the system is promoted due to a higher number of interfaces. Authors such as J.C. Caicedo et al. [22] also showed this behavior in multilayer systems. In addition, the roughness is a factor that influenced the tribological properties, influencing the formation of asperities, the type of contact and the wear generated at the beginning of the tribological test [23, 24].

3.3.2 Morphological study for TiCN, BCN and CrAlN coatings nitride coatings

Using SPIP® statical analysis software, AFM images were obtained in contact mode (**Figure 7a–c**). From these images, the surface roughness and grain size values of each coating were obtained (**Figure 8a** and **b**). From these images it can be clearly observed the change in surface morphology as the nature of the coating changes, taking into account that the three materials have a similar thickness.

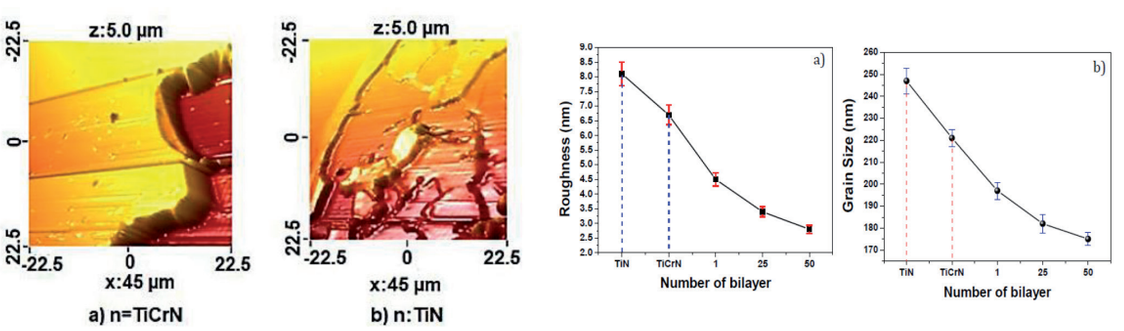

Figure 6.
Atomic force microscopy for single layer coatings: (a) TiCrN and (b) TiN.

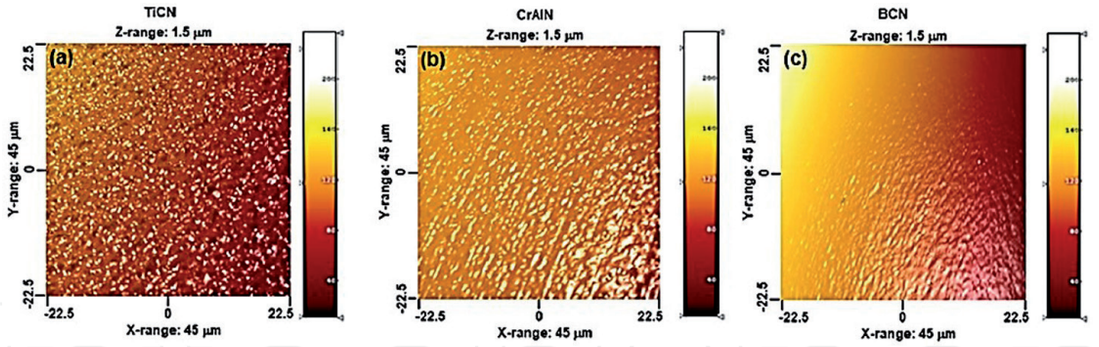

Figure 7.
AFM images for all coatings: (a) TiCN, (b) CrAlN and (c) BCN.

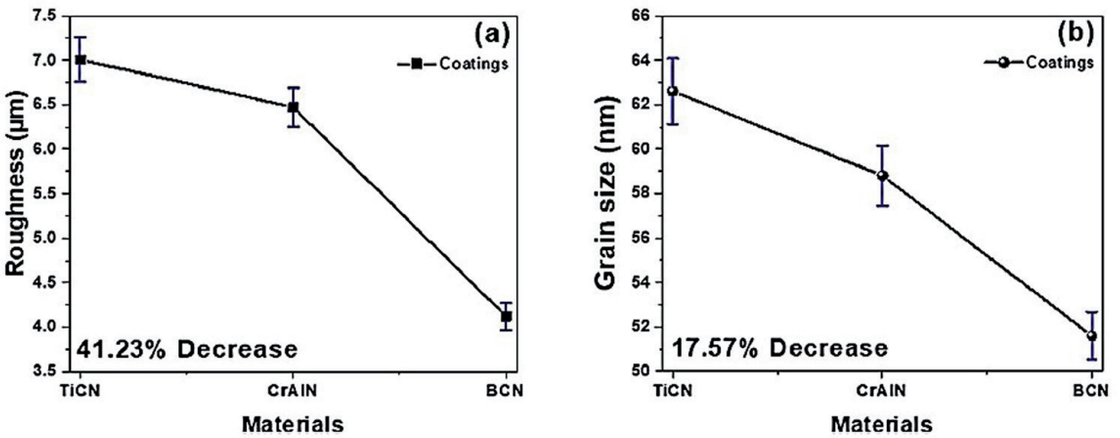

Figure 8.
Influence of TiCN, BCN and CrAlN coatings' nature on morphological surface: (a) roughness as a function of coating materials, (b) grain size as a function of coating materials.

Figure 8 shows the relationship between surface roughness and grain size. These results indicated that the TiCN coating presented the higher values for roughness = 7.01 µm and grain size = 62.6 µm; followed by the CrAlN coating, which presented roughness = 6.47 µm and grain size = 58.8 µm. Finally, the BCN coating presented the best characteristics (lowest values) of roughness = 4.12 µm and grain size = 51.6 µm. Thus, there was a decrease of 41.23% and 17.57% for roughness and grain size respectively. From the results obtained by AFM, it was observed that the BCN coating presented the best results, which is due to the susceptibility of BCN to grow with low roughness on the substrate with respect to the other coatings, also producing the reduction of the grain size (which is directly proportional to the reduction of the roughness), causing a more compact coating to be generated.

3.3.3 Morphological study for Si_3N_4 coatings nitride coatings

Figure 9 presents the AFM images of the Si3N4 coating, where it was determined that the coating presented a grain morphology with circular geometry with a low grain size and a homogeneous surface. This surface characteristic is attributed to a high ionic bombardment of Ar+ atoms generated during the deposition process, which modifies the surface morphology of the coating. Thus, ion bombardment causes an increase in the energy of the atoms adsorbed on the substrate surface, generating an increase in the nucleation sites. This results in a reduction of grain size, roughness and columnar growth, as well as an increase in the density of the coatings [5, 25]. **Figure 9b** shows the values of the roughness and grain size for

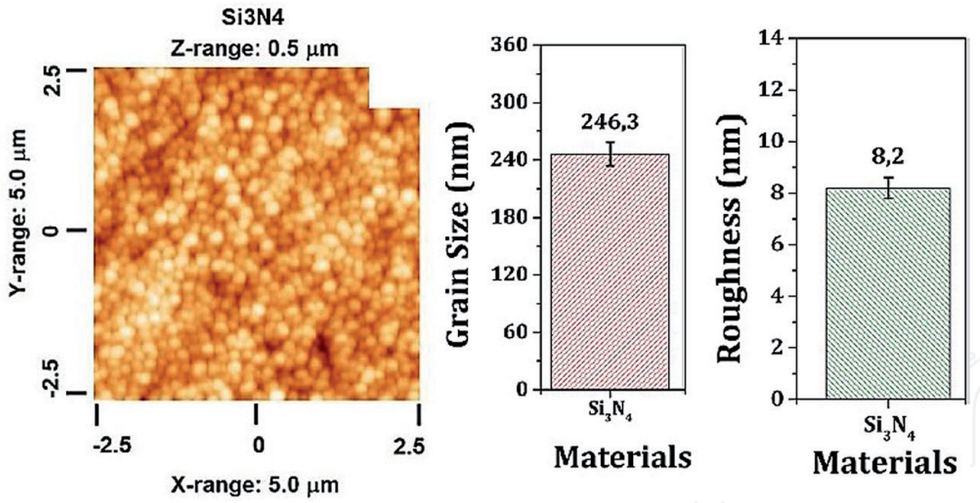

Figure 9.
Atomic force microscopy (AFM) images for the single layer Si_3N_4 coatings, showing the morphological analysis of the Si_3N_4 coatings: roughness and grain size.

the coating, where it was determined that the Si3N4 surface presented optimal results, so these morphological characteristics will greatly affect the mechanical and tribological properties of this coating.

3.4 Mechanical properties comparison between nitride coatings

3.4.1 Mechanical properties for TiN and TiCrN nitride coatings

Figure 10 shows the load-depth curves obtained during the nanoindentation test fir the TiN and TiCrN single layer coating and the TiN/TiCrN multilayer system as a function of the bilayers number. These results showed a higher penetration fir the substrate (steel H13). In addition, the TiCrN layer showed a lower penetration compared to the TiN layer and for the multilayer system, there was a decrease in penetration as the bilayers number increased. This behavior is due to the surface properties of each coating as corroborated in the **Figure 10b** and **c**. Thus, **Figure 10b** and **c** shows the values of hardness (H) and elastic modulus (E) for the individual coating and multilayers system (TiN, TiCrN and [TiN/TiCrN]) where it was determined that both presented hardness higher than 10 Gpa, which serves as a parameter to qualify them as hard coatings, which allows to have a longer life time and lower wear rates in cutting tools that implement this type of coatings [26]. Finally, these results show a hardness of 18.5 Gpa and an elastic modulus 284.17 Mpa, as well as a hardness of 20.35 Gpa and elastic modulus 314.2 Mpa for the TiN and TiCrN single layers, respectively.

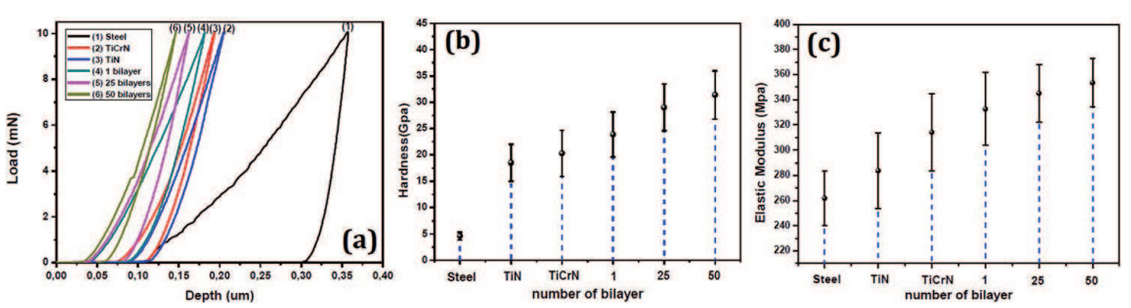

Figure 10.
Nanoindentation results (a) Load-displacement curves for the TiN and TiCrN single layers; (b) Hardness and (c) Elastic modulus values.

The TiCrN single layer showed better properties due to the higher compressive stresses generated in the coating during the sputtering of the deposition process [22].

3.4.2 Mechanical properties for TiCN, BCN and CrAlN coatings nitride coatings

After the structural and morphological studies presented above, the mechanical properties of TiCN, CrAlN and BCN coatings deposited on AISI 1045 steel substrates presented in the **Figure 11a** were analyzed by means of load-displacement curves. **Figure 11b** and **c** show the hardness and elastic modulus of the coatings, where values were obtained for TiCN (H = 28 Gpa, E=224 Mpa), followed by CrAlN (H=30 Gpa, E=251 Gpa= and then BCN (H=33 Gpa, E=335 Gpa). These results obtained are attributed to surface factors such as those presented by AFM (**Figure** 7), where a direct relationship between the roughness and grain size is show. Thus, having a smaller grain size results in a higher grain edge density and these grain edges act as impediments to the movement of dislocations. Thus, higher shear stresses are required for the dislocations to pass through these obstacles, so these coatings will have better mechanical properties [27–30]. On the other hand, the elastic modulus (E) of coatings is related to the type of material, but not to its microstructure; in this sense the elastic modulus (E) depends on its crystalline structure and microstructural factors such as the lattice parameter.

3.4.3 Mechanical properties for Si_3N_4 coatings nitride coatings

Figure 12 shows the results of hardness (H) and reduced elastic modulus (Er) of the Si3N4 coating deposited on an AISI 316 steel. Through these results it was possible to determine that this coating presented a higher resistance to being indented in comparison to the Al2O3 coating. This behavior is attributed to surface factors such as a smaller grain size, which means an increase in the amount of grain boundaries, which act as impediments to the displacement of dislocations. On the other hand, the presence of compressive stresses generated during the deposition process contributed to the increase in the hardness of this coating. Thus, the Si3N4 coating obtained the best mechanical properties such as hardness (H) and reduction elastic modulus (Er).

3.5 Tribological properties comparison between nitride coatings

3.5.1 Tribological properties for TiN and TiCrN nitride coatings

Figure 13 shows the tribological behavior of individual TiN and TiCrN coatings as well as the [TiN/TiCrN] multilayer system as a function of the bilayers number.

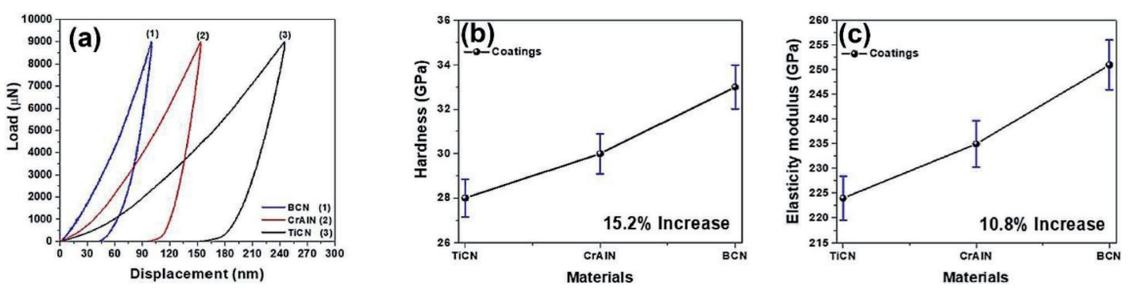

Figure 11.
Nanoindentation results: (a) Load-displacement curves for the TiCN, CrAlN and BCN single layers, (b) Hardness and (c) Elastic modulus values.

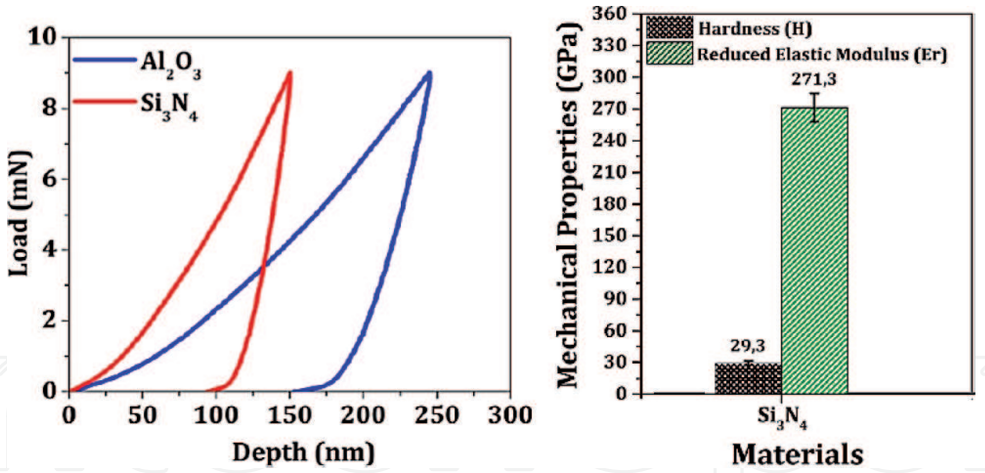

Figure 12.
Load-depth curves for the Si3N4 coatings and mechanical properties as a function of the material: hardness and reduced modulus of elasticity Si_3N_4 coatings.

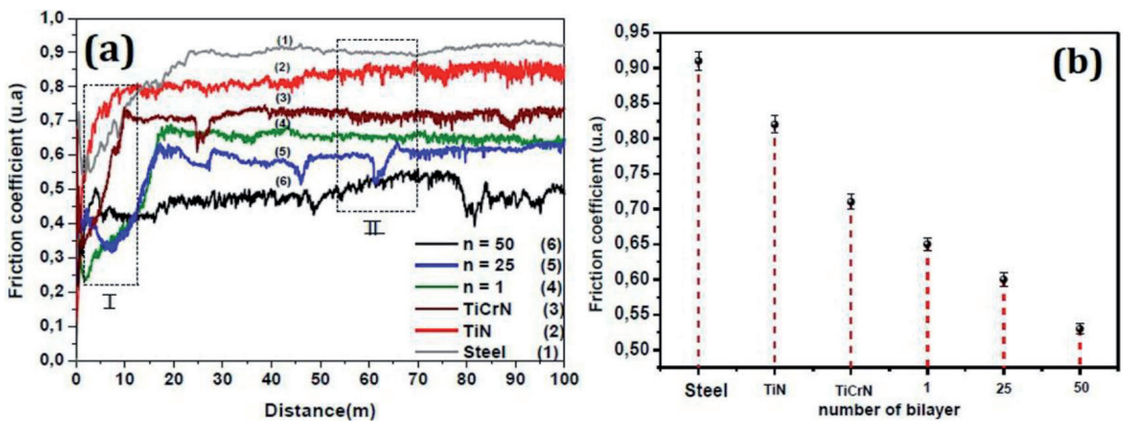

Figure 13.
Tribological study of single layer coatings [TiN and TiCrN] and multilayer system [TiN/TiCrN]n as a function of the bilayers number (a) Friction coefficient versus distance and (b) Friction coefficient values for single layer [TiN and TiCrN] and multilayer system [TiN/TiCrN]n.

Through this behavior, two characteristics stages were identified. Stage I, known as the starting period, where there is a rapid increase in the friction coefficient due to the direct contact between the asperities and the counterpart (Steel 440), in this way, these asperities are eliminated and deformed. Stage II, known as running-in, in which the deformation of the asperities is maintained together with the appearance of defects of the coating, leading to the formation of wear particles or debris [24]. **Figure 13b** show the value of the friction coefficient in the stabilization stage. From this result, it is evident that the TiCrN coating showed a decrease compared to the TiN coating, this decrease in the coefficient is attributed to the deformation of the crystalline structure by the incorporation of chromium atoms, which modifies its surface and mechanical properties, as show above (**Figures 6** and **10**). Furthermore, this tribological behavior can be related to the mechanical friction model proposed by Archad, where the friction coefficient of each coating depends on surface factors such as roughness R(s,a), and elastic–plastic properties (hardness H, or elastic modulus Er). By means of this model, it is established that when the surface of the coating has a low roughness (**Figure 6**) and a high hardness (**Figure 10**) the friction coefficient will be lower since there will be less wear on the surface [31].

The study of the adhesion of coatings was carried out by means of the scratch teste. For this, **Figure 14a** and **b** show the behavior of TiN and TiCrN coatings

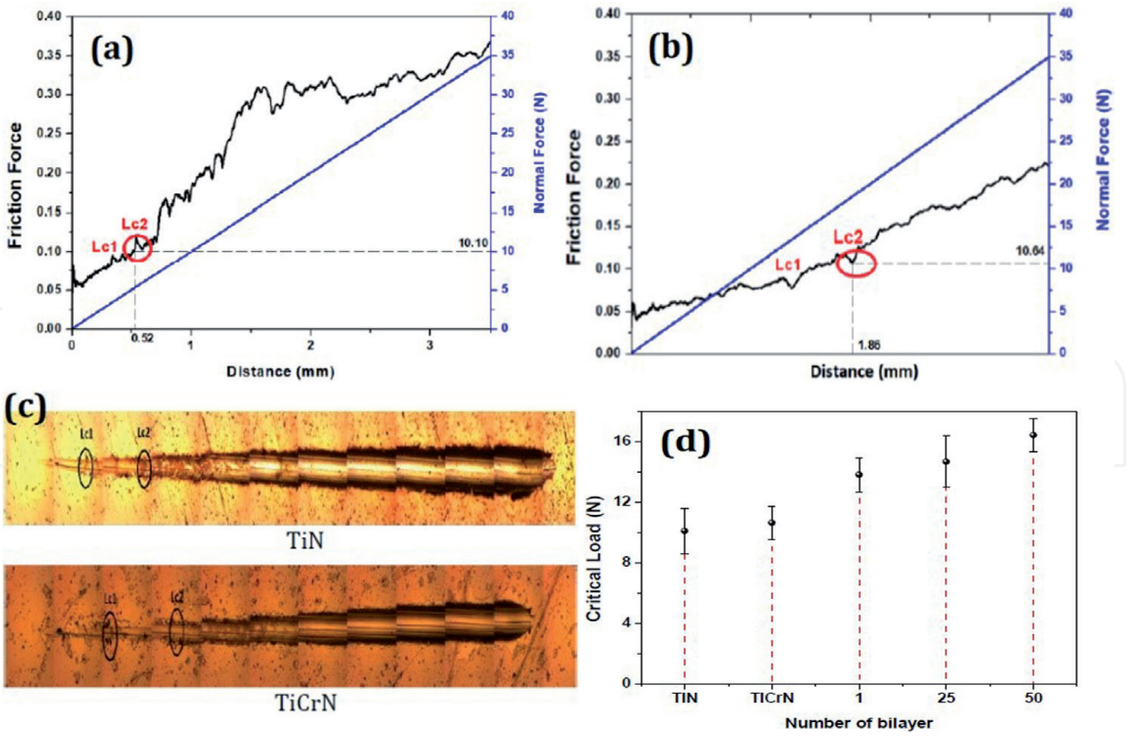

Figure 14.
Friction coefficient and normal strength versus distance and critical load Lc2 for single layers (TiN and TiCrN) and optical micrographs of the wear track of the dynamic scratch test at a resolution of x10.

respectively, where two characteristics stages known as (Lc1 and Lc2) could be characterized. Lc1, is known as the cohesive failure where the first cracks or first failure in the coating start to occur and Lc2 known as the adhesive type failure where delamination occurs at the edge of the scratch track presented in **Figure 14c**. In addition, **Figure 14a** and **b** show the adhesion strength for the single layer coatings as a function of Lc1 and Lc2 failures, where the change in slope corresponding to the adhesive and cohesive failure are observed. Thus, there results were corroborated with the micrographs of the wear tracks of each test where the morphological changes suffered by the surface due to the cohesive and adhesive failure can be appreciated [32].

Finally, **Figure 14d** show the value of the critical load (Lc2) for the TiN and TiCrN single layer coatings as well as the multilayer system [TiN/TiCrN] as a function of the bilayers number. From these results it was possible to show that the TiCrN coating presented a higher resistance to be delaminated, this increase of the Lc2 load in comparison to the TiN coating is attributed to physical factors, such as the change produced within its crystalline structure by the incorporation of chromium atoms in its structure as corroborated in **Figure 1**. This change in the crystalline structure due to the increase of compressive stresses generated that a higher amount of external energy is required to cause a delamination of the coating. In addition, for the multilayer system, it was determined that the increase in the number of interfaces directly affects the delamination resistance of the coatings, because the interfaces restrict movement of the cracks through the coating.

3.5.2 Tribological properties for TiCN, BCN and CrAlN coatings nitride coatings

Figure 15 show the tribological behavior of TiCN, BCN and CrAlN coatings deposited on AISI 1045 steel substrate when in direct contact with a 100Cr6 steel counterpart in lubricated and non-lubricated environments. These results showed two characteristic stages, stage I, known as the starting period, which is related to the

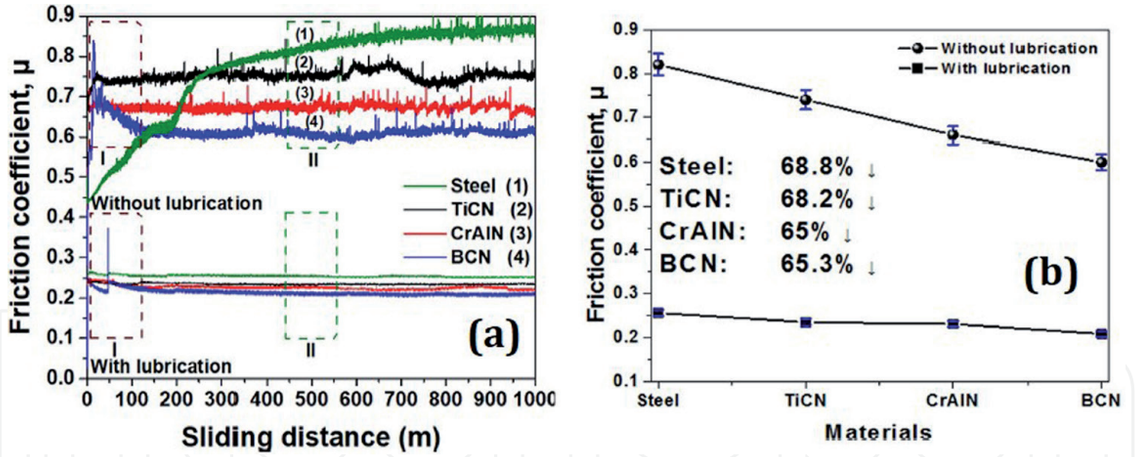

Figure 15.
Tribological results of the AISI 1045 steel substrates with TiCN, BCN and CrAlN single layer coatings with and without lubrication: friction coefficient as a function of the sliding distance and friction coefficient for different coatings (TiCN, CrAlN and BCN): without lubrication and with lubrication.

interference of the friction mechanism due to the initial surface contact associated with the surface and counterpart; therefore; this contact generated a rapid increase in the friction coefficient and stage II is characterized by the friction coefficient presents a settlement period, where a deformation and elimination of the asperities takes place, causing a stabilization of the friction coefficient. Thus, at the settling distance there is an equilibrium of the friction coefficient in relation to the adhesive and interferential friction mechanisms. Therefore, the value of the friction coefficient will depend on the predominant effect related to the adhesive and interferential mechanisms. Finally, **Figure 13b** shows the value of the friction coefficient for all coatings and substrate (AISI 1045) in the non-lubricated environment, where they were obtained for Substrate = 0.82; TiCN = 0.74; CrAlN = 0.66 and BCN = 0.6. On the other hand, the values of the friction coefficient obtained in a lubricated environment were Substrate = 0.26; TiCN = 0.24; CrAlN = 0.23 and BCN = 0.21. Taking into account the last result, it was established that the BCN coating presented the best tribological behavior for both environments (dry and lubricated), this good behavior is attributed to its surface and mechanical properties presented above.

Through the results obtained by the scratch test presented in **Figure 16**, it was possible to evidence an increase of the critical load (Lc2) as a function of the nature of the coating (TiCN, CrAlN and BCN). Moreover, the change of the critical load is related to the increase of the mechanical properties of the coatings (**Figure 11**), the reduction of the surface roughness (**Figures 7** and **8**) and the reduction of the friction coefficient (**Figure 15**). In addition, factor such as resistance to plastic

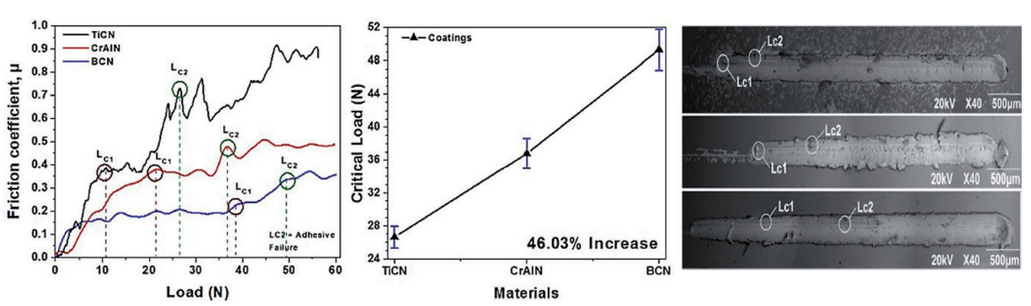

Figure 16.
Friction coefficient as a function of the applied load for all TiCN, BCN and CrAlN coatings showing the cohesive failure (L_{C1}) and adhesive failure (L_{C2}) and critical load as a function of the coating's nature (TiCN, BCN and CrAlN).

deformation and elastic recovery prevent the propagation and displacement of cracks through the coating, thus requiring a higher applied external load to cause failure between the coating and the substrate (adhesive failure). Therefore, an increase in the critical adhesive load (Lc2) of 46.03% was found for the boron carbide nitride (BCN) coating relative to the coating with lower mechanical properties (TiCN).

3.5.3 Tribological properties for Si_3N_4 coatings nitride coatings

Figure 17a shows the friction coefficient of Si_3N_4 based coating deposited on AISI 316 steel substrates in a lubricated and dry environment. The results of the tribological study in dry environment evidenced two characteristic stages during the test. Stage I, known as the starting period, is associated with the interferential friction mechanism due to the direct contact between the surface roughness of the coating and the counterpart (100Cr6 steel), whereby, which, the roughness decreases and generates wear particles on the surface [5]. These particles cause a rapid increase in the friction coefficient followed by a slight decrease until it stabilizes. Subsequently, in stage II, the reduction of these roughness is maintained along with the appearance of new defects in the coating, leading to a stabilization of the friction coefficient [33].

In the lubricated environment, the curves show a different behavior in relation to the tribological study in dry environment (not lubricated), since the incorporate of the lubricant inside the tribological contact generated a large decrease in the friction coefficient. Therefore, the decrease in the friction coefficient is attributed to the fact that the lubricant supports the applied external load, decreasing the roughness reduction and caused a lower amount of wear particles (debris) on the tribo-system surface. **Figure 17b** shows the value of the friction coefficient as a function of the material, in dry and lubricated environment. This behavior is related to the friction model proposed by Archad [31]. This model correlates the mechanical (H, Er) and morphological (roughness) properties of the coating, where surface with better mechanical properties and lower roughness will present a lower friction coefficient, as was the case for the Si_3N_4 coating. This is due to the fact that the Si_3N_4 coating is able to withstand the continuous passage of the counterpart in relation to the uncoated steel substrate, thus producing a lower wear rate on its surface.

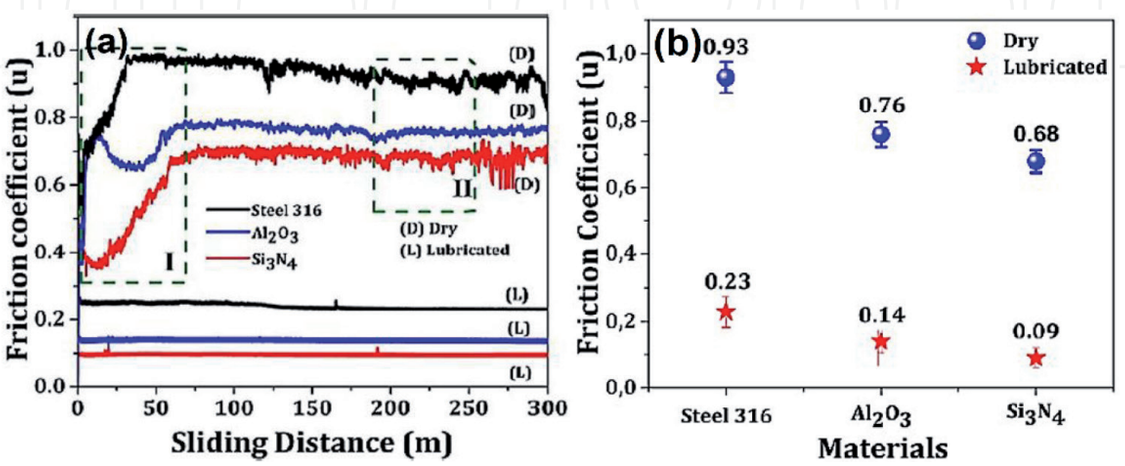

Figure 17.
Friction coefficient for Si_3N_4 coatings in lubricated and non-lubricated environment: (a) friction coefficient versus sliding distance (b) friction coefficient as a function of the material evaluated.

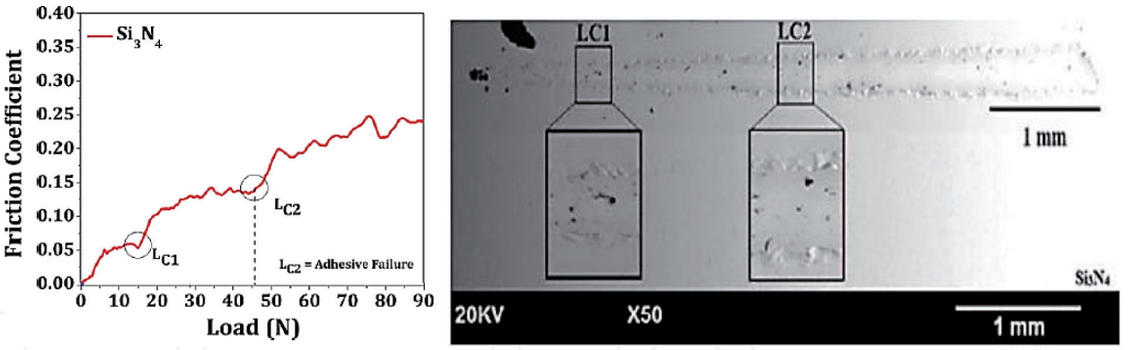

Figure 18.
SEM micrographs of the wear tracks generated in the scratch test for Si_3N_4 coatings deposited on 316 stainless steel substrates.

Figure 18 shows the friction coefficient as a function of critical load for Si_3N_4 coating, in addition to the SEM micrograph of the scratch track where the types of failures, cohesive failure (Lc1) and adhesive failure (Lc2), were determined. In the cohesive failure (Lc1) the first cracks are produced by the applied external load, and in the adhesive failure (Lc2) a delamination is generated at the edge of the scratch track. These tribological characteristics are due to the mechanical and surface properties of the coating.

4. Conclusions

From the study of the mechanical and tribological behavior of TiN and TiCrN coating. It was determined that the TiCrN coating presented the best set of properties, these better properties were attributed to the incorporation of chromium (Cr) atoms within the crystalline structure of TiN. Therefore, structural, morphological and mechanical changes were produced, which influenced its behavior under applied load states.

The above results determined that the boron nitride (BCN) coating had the lowest friction coefficient (0.208) in a lubricated environment and had a friction coefficient of 0.6 in a non-lubricated environment. This tribological behavior is associated with its low roughness and high mechanical properties with respect to the coatings (TiCN and CrAlN). In this research, a decrease in the friction coefficient was obtained comparing non-lubricated and lubricated environments by 68.2%, 65% and 65.3% for TiCN, CrAlN and BCN coatings, respectively. On the other hand, cohesive failure (Lc1) and adhesive failure (Lc2) were obtained for BCN coating with 38.41 N and 49.32 N, respectively.

The tribological properties analyzed by Pin On Disk in dry and lubricated environment for the Si_3N_4 coating presented the lowest friction coefficient in relation to uncoated steel. This behavior is attributed to its structural, mechanical and morphological properties, so the Si_3N_4 coating proved to be a suitable candidate to be implemented in the food and pharmaceutical industry.

Acknowledgements

This research was supported by Universidad Militar Nueva Granada, Bogotá, Colombia; CIC biomaGUNE, San Sebastian, Spain; Centro de Desarrollo Tecnológico y Asistencia Técnica a la Industria del Servicio Nacional de Aprendizaje (CDT-ASTIN-SENA), Cali, Colombia; Universidad Autónoma de Occidente, Cali, Colombia.

DOI: http://dx.doi.org/10.5772/intechopen.100629

Author details

Christian Ortiz Ortiz*, Erick Hernandez-Rengifo and Julio Cesar Caicedo
Universidad del Valle, Cali, Colombia

*Address all correspondence to: christian.ortiz.ortiz@correounivalle.edu.co

References

[1] Grigoriev S, Vereschaka A, Milovich F, Tabakov V, Sitnikov N, Andreev N, et al. Investigation of multicomponent nanolayer coatings based on nitrides of Cr, Mo, Zr, Nb, and Al. Surf. Coatings Technol. 2020;**401**:126258 https://doi.org/10.1016/j.surfcoat.2020.126258

[2] Hacisalihoglu I, Yildiz F, Alsaran A. Wear performance of different nitride-based coatings on plasma nitrided AISI M2 tool steel in dry and lubricated conditions. Wear. 2017;**384-385**:159-168 https://doi.org/10.1016/j.wear.2017.01.117

[3] Chauhan KV, Rawal SK. A Review Paper on Tribological and Mechanical Properties of Ternary Nitride based Coatings. Procedia Technol. 2014;**14**:430-437 https://doi.org/10.1016/j.protcy.2014.08.055

[4] Kumar S, Maity SR, Patnaik L. Effect of heat treatment and TiN coating on AISI O1 cold work tool steel. Mater. Today Proc. 2019;**26**:685-688 https://doi.org/10.1016/j.matpr.2019.12.367

[5] Ortiz CH, Colorado HD, Aperador W, Jurado A. Influence of the number of bilayers on the mechanical and tribological properties in [TiN/TiCrN]n multilayer coatings deposited by magnetron sputtering. Tribol. Ind. 2019;**41**:330-343 https://doi.org/10.24874/ti.2019.41.03.03

[6] Ortiz CH, Hernandez-Rengifo E, Guerrero A, Aperador W, Caicedo JC. Mechanical and tribological properties evolution of [si3n4/al2o3]n multilayer coatings. Tribol. Ind. 2021;**43**:23-39 https://doi.org/10.24874/ti.952.08.20.01

[7] Chen R, Tu JP, Liu DG, Mai YJ, Gu CD. Microstructure, mechanical and tribological properties of TiCN nanocomposite films deposited by DC magnetron sputtering. Surf. Coatings Technol. 2011;**205**:5228-5234 https://doi.org/10.1016/j.surfcoat.2011.05.034

[8] Correa JF, Aperador W, Caicedo JC, Alba NC, Amaya C. Structural, mechanical and tribological behavior of TiCN, CrAlN and BCN coatings in lubricated and non-lubricated environments in manufactured devices. Mater. Chem. Phys. 2020;**252**:123164 https://doi.org/10.1016/j.matchemphys.2020.123164

[9] Hernandez-Rengifo EH-R, Ortiz CH, Hidalgo CH, Ballesteros JA, Caicedo JC. Comparative Study of Tribological and Mechanical Properties Between Single Layers of Al2O3 and Si3N4 Deposited on AISI 316 Stainless Steel. Tribol. Ind. 2021;**43**:259-273 https://doi.org/10.24874/ti.956.09.20.01

[10] Paksunchai C, Denchitcharoen S, Chaiyakun S, Limsuwan P. Growth and Characterization of Nanostructured TiCrN Films Prepared by DC Magnetron Cosputtering. J. Nanomater. 2014;**2014**:1-9 https://doi.org/10.1155/2014/609482

[11] Hovsepian PE, Ehiasarian AP, Petrov I. Structure evolution and properties of TiAlCN/VCN coatings deposited by reactive HIPIMS. Surf. Coatings Technol. 2014;**257**:38-47 https://doi.org/10.1016/j.surfcoat.2014.07.065

[12] Correa JF, Aperador W, Caicedo JC, Alba NC, Amaya C. Structural, mechanical and tribological behavior of TiCN, CrAlN and BCN coatings in lubricated and non-lubricated environments in manufactured devices. Mater. Chem. Phys. 2020;**252**:123164 https://doi.org/10.1016/j.matchemphys.2020.123164

[13] Wu Z, Li S, Xu Z, Wang Q, Zhou F. Tribological properties of boron carbonitride coatings sliding against

different wood (acerbic, beech, and lauan) balls. Adv. Compos. Lett. 2019;**28**:1-10 https://doi.org/10.1177/0963693519875737

[14] Falsafein M, Ashrafizadeh F, Kheirandish A. Influence of thickness on adhesion of nanostructured multilayer CrN/CrAlN coatings to stainless steel substrate. Surfaces and Interfaces. 2018;**13**:178-185 https://doi.org/10.1016/j.surfin.2018.09.009

[15] Caicedo JC, Aperador W, Mozafari M, Tirado L. Evidence of Electrochemical Resistance on Ternary V-C-N Layers. Silicon. 2018;**10**:2499-2507 https://doi.org/10.1007/s12633-018-9782-7

[16] Vyas A, Li KY, Zhou ZF, Shen YG. Synthesis and characterization of CNx/TiN multilayers on Si(100) substrates. Surf. Coatings Technol. 2005;**200**: 2293-2300 https://doi.org/10.1016/j.surfcoat.2004.10.015

[17] Nocua JE, Morell G, Piazza F, Weiner BR. Synthesis and characterization of stoichiometric boron nitride nanostructures | Síntesis y caracterización de nanoestructuras estequiométricas de nitruro de boro. Superf. y Vacio. 2012;**25**:194-198

[18] L. Ipaz, W. Aperador, J. Caicedo, J. Esteve, G. Zambrano, A Practical Application of X-Ray Spectroscopy in Ti-Al-N and Cr-Al-N Thin Films, in: X-Ray Spectrosc., InTech, 2012. https://doi.org/10.5772/29640.

[19] Hu H, Carim AH. Determination of attenuation lengths and electron escape depths in silicon nitride thin films. J. Electrochem. Soc. 1993;**140**:3203

[20] Kishi K, Roberts MW. Adsorption of nitrogen and ammonia by polycrystalline iron surfaces in the temperature range 80-290 K studied by electron spectroscopy. Surf. Sci. 1977;**62**:252-266 https://doi.org/10.1016/0039-6028(77)90441-1

[21] Shin SH, Cho JW, Kim SH. Structural investigations of CaO-CaF2-SiO2-Si3N4 based glasses by Raman spectroscopy and XPS considering its application to continuous casting of steels. Mater. Des. 2015;**76**:1-8 https://doi.org/10.1016/j.matdes.2015.03.035

[22] Caicedo JC, Cabrera G, Caicedo HH, Amaya C, Aperador W. Nature in corrosion-erosion surface for [TiN/TiAlN]n nanometric multilayers growth on AISI 1045 steel. Thin Solid Films. 2012;**520**:4350-4361 https://doi.org/10.1016/j.tsf.2012.02.061

[23] Navarro-Devia JH, Amaya C, Caicedo JC, Aperador W. Performance evaluation of HSS cutting tool coated with hafnium and vanadium nitride multilayers, by temperature measurement and surface inspection, on machining AISI 1020 steel. Surf. Coatings Technol. 2017;**332**:484-493 https://doi.org/10.1016/j.surfcoat.2017.08.074

[24] Piedrahita WF, Aperador W, Caicedo JC, Prieto P. Evolution of physical properties in hafnium carbonitride thin films. J. Alloys Compd. 2017;**690**:485-496

[25] Ipaz L, Caicedo JC, Esteve J, Espinoza-Beltran FJ, Zambrano G. Improvement of mechanical and tribological properties in steel surfaces by using titanium-aluminum/titanium-aluminum nitride multilayered system. Appl. Surf. Sci. 2012;**258**:3805-3814 https://doi.org/10.1016/j.apsusc.2011.12.033

[26] Donnet C, Erdemir A. Historical developments and new trends in tribological and solid lubricant coatings. Surf. Coatings Technol. 2004;**180-181**:76-84 https://doi.org/10.1016/j.surfcoat.2003.10.022

[27] Choi EY, Jang CS, Kang MC, Kim KH. Synthesis and Characterization of

$Ti\text{-}C_x\text{-}N_{1-x}$ Coatings Prepared by Arc Ion Plating. Solid State Phenom. 2006;**118**:311-316 https://doi.org/10.4028/www.scientific.net/SSP.118.311

[28] Caicedo JC, Amaya C, Yate L, Gómez ME, Zambrano G, Alvarado-Rivera J, et al. TiCN/TiNbCN multilayer coatings with enhanced mechanical properties. Appl. Surf. Sci. 2010;**256**:5898-5904 https://doi.org/10.1016/j.apsusc.2010.03.071

[29] J.E. Sanchéz, O.M. Sanchéz, L. Ipaz, W. Aperador, J. Caicedo, C. Amaya, M.A. Landaverde, F.J. Espinoza-Beltrán, J. Muñoz-Saldaña, G. Zambrano, Mechanical, tribological, and electrochemical behavior of Cr1−xAlxN coatings deposited by r.f. reactive magnetron co-sputtering method, Appl. Surf. Sci. 256 (2010) 2380-2387. https://doi.org/10.1016/j.apsusc.2009.10.071.

[30] Barshilia HC, Deepthi B, Rajam KS. Deposition and characterization of CrN/Si3N4 and CrAlN/Si3N4 nanocomposite coatings prepared using reactive DC unbalanced magnetron sputtering. Surf. Coatings Technol. 2007;**201**:9468-9475 https://doi.org/10.1016/j.surfcoat.2007.04.002

[31] Archard JF. Contact and Rubbing of Flat Surfaces. J. Appl. Phys. 1953;**24**:981-988. https://doi.org/10.1063/1.1721448.

[32] Caicedo JC, Aperador W, Amaya C. Determination of physical characteristic in vanadium carbon nitride coatings on machining tools. Int. J. Adv. Manuf. Technol. 2017;**91**:1227-1241 https://doi.org/10.1007/s00170-016-9835-2

[33] Piedrahita WF, Aperador W, Caicedo JC, Prieto P. Evolution of physical properties in hafnium carbonitride thin films. J. Alloys Compd. 2017;**690**:485-496 https://doi.org/10.1016/j.jallcom.2016.08.109